Inorganica Chimica Acta 567 (2024) 122066

Contents lists available at ScienceDirect

Inorganica Chimica Acta

journal homepage: www.elsevier.com/locate/ica

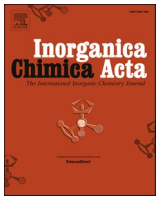

Research paper

Lanthanide furoate complexes as promising systems with double effects – From suppression of mycobacteria to potential bioimaging

Marina A. Uvarova [a,1,*], Marina E. Nikiforova [a], Maxim A. Shmelev [a], Teimur M. Aliev [b], Mikhail T. Metlin [c], Ilya V. Taydakov [c], Olga B. Bekker [d], Oleg A. Levitskiy [e], Tatiana V. Magdesieva [e], Gennady L. Rusinov [f,g], Danila V. Belyaev [f,g], Diana V. Vakhrusheva [f], Svetlana Yu. Krasnoborova [f], Mikhail A. Kiskin [a], Irina A. Lutsenko [a], Igor L. Eremenko [a]

[a] N.S. Kurnakov Institute of General and Inorganic Chemistry, Russian Academy of Sciences, Leninsky Prosp. 31, 119991 GSP-1 Moscow, Russian Federation
[b] A.N. Nesmeyanov Institute of Organoelement Compounds, Russian Academy of Sciences, Vavilova Str. 28, 119991 Moscow, Russian Federation
[c] P.N. Lebedev Physical Institute, Russian Academy of Sciences, Leninsky Prosp. 53, 119991 Moscow, Russian Federation
[d] Vavilov Institute of General Genetics, Russian Academy of Sciences, Gubkina, 3, 119333 Moscow, Russian Federation
[e] Lomonosov Moscow State University, Dept. of Chemistry, Leninskie Gory 1/3, Moscow 119991, Russian Federation
[f] National Medical Research Center of Phthisiopulmonology and Infection Diseases, 22 Parts'ezda St., 50, Ekaterinburg 620039, Russian Federation
[g] Postovsky Institute of Organic Synthesis, Ural Branch of the Russian Academy of Sciences, S. Kovalevskoy Str., 22, Ekaterinburg 620137, Russian Federation

ARTICLE INFO

Keywords:
Furoate complexes
Rare earth element complexes
Crystal structure
Anti-tuberculosis activity
Luminescence
Chromophores
Bioimaging

ABSTRACT

Several ternary complexes of rare earth ions (Gd^{3+}, Eu^{3+}, Sm^{3+}) with 3-furoic (H3fur) / 5-nitro-2-furoic (Hnfur) acids and 1,10-phenanthroline (phen) have been synthesized. According to the X-ray data the resulting complexes can be divided into two groups – heterocarboxylate $[Ln_2(3fur)_4(OAc)_2(phen)_2]\cdot L$ and homocarboxylate complexes $[Ln_2(nfur)_6(phen)_2]\cdot L$ (Ln^{III} = Gd (**1**, **2**), Eu (**3**, **4**), Sm (**5**, **6**, **7**); L = 4EtOH (**1**–**4**), 4MeOH (**5**), H_2O (**7**)). The stability of the complexes **1**–**6** in solutions was studied by recording electronic absorption spectra for two days. Optical properties of the complexes **1**–**6** were studied by recording absorption, excitation and luminescence spectra. The study of antibacterial properties **1**–**7** showed high activity of complexes *in vitro* against non-pathogenic *Mycolicibacterium smegmatis*. For the most active **3**, antibacterial activity against the reference strain *Mycobacterium tuberculosis* H37Rv was determined (minimum inhibitory concentration (MIC) up to 12.5 μg/mL).

1. Introduction

The fight against infectious diseases remains one of the most important issues in medicine. Though numerous antibacterial drugs are used in the therapy of diseases, the development of various types of resistance to many drugs by bacteria remains the main problem, so an incessant search for new antibacterial drug components is ongoing. Studies performed in recent years show the prospects of using metal-containing drugs in medicine: iron and cobalt preparations for the treatment of various types of anemia; antiparasitic, antimicrobial and antiseptic compounds of zinc, silver, and mercury; platinum complexes as anticancer drugs; complexes of gadolinium, samarium, etc. in diagnostics [1–6]. At present, the search for compounds that can simultaneously "work" in different directions ("multitarget effect") – for example, inhibit bacterial activity and detect the focus of inflammation or drug localization – is an important direction. In view of this, one of the possible solutions to the problem may lie in the development of biologically active substances with pronounced photoluminescent properties for bioimaging. A number of requirements for real application in therapy should be met: they should have low toxicity, be stable under physiological conditions, have good photophysical parameters, etc.

Rare earth metals are promising complexing agents for the creation of photo- and bioactive compounds, since trivalent lanthanide ions exhibit ubiquitous luminescence due to their unique f-electronic structure [7–10]. A significant increase in luminescence can be achieved due to the antenna effect due to the transfer of absorbed energy by

* Corresponding author.
E-mail address: yak_marin@mail.ru (M.A. Uvarova).
[1] Foundation item: Project supported by Russian Science Foundation (24–23-00188)

https://doi.org/10.1016/j.ica.2024.122066
Received 14 March 2024; Received in revised form 4 April 2024; Accepted 11 April 2024
Available online 12 April 2024

polydentate ligands to the lanthanide ion [11–12]. In the series of lanthanides, complexes with Eu^{3+}, Tb^{3+}, Gd^{3+}, and Sm^{3+} ions are stable and feature good photophysical characteristics, which is of particular interest for their use as luminescent probes in the clinical diagnostics [13–18]. Moreover, a number of studies have demonstrated the antibacterial activity of lanthanide complexes [19–21]. It has also been proved that compounds containing lanthanide(III) ions, such as Nd^{3+}, Sm^{3+} or Yb^{3+}, can be used for in vivo luminescent imaging due to emission in the near-infrared region, which can be detected through animal tissues of considerable thickness [22]. Both the luminescent and antibacterial properties of lanthanide complexes are determined by the choice of ligands. Carboxylate anions have ample coordination capabilities and can form complexes of various sizes owing to their structure [23–25]. The incorporation of aromatic substituents, such as furan and its derivatives, as well as oligopyridines, into a carboxylate anion enhance many properties of the complexes, such as biological, photophysical, and magnetic ones [26–36].

This work presents synthetic approaches to the preparation of Eu^{III}, Gd^{III} and Sm^{III} complexes with 3-furoic or 5-nitro-2-furoic acids and 1,10-phenanthroline anions and to a study of the *in vitro* activity of these complexes against the nonpathogenic strain *Mycolicibacterium smegmatis*, which is used as a model organism for the slow-growing bacteria *M. tuberculosis* (Koch's bacillus) and for the primary screening of antituberculosis drugs. For compound **3**, which showed the highest activity against *M. smegmatis*, the *in vitro* antibacterial activity against the reference strain *M. tuberculosis* H37Rv was determined. The stability of complexes **1–6** was confirmed by UV–vis spectroscopy upon dissolution in physiological 0.9 % NaCl solution and 5 % glucose solution. The optical properties of solid state samples **1–6** were studied by recording their absorption, excitation and luminescence spectra.

2. Experimental

2.1. Materials and methods

Commercial reagents and solvents were used for the synthesis: 3-furoic acid (H3fur, 99 %), 5-nitro-2-furoic acid (Hnfur, 99 %), $Sm_2(CO_3)_3{\cdot}4H_2O$ (≥99 %), $Eu(OAc)_3{\cdot}3H_2O$ (≥99 %), $Gd(OAc)_3{\cdot}3H2O$ (≥99 %), $Sm(OAc)_3{\cdot}3H_2O$ (≥99 %), acetonitrile (≥99 %), ethanol (96 %), methanol (96 %), 1,10-phenanthroline (phen, 99 %).

The IR spectra of the compound were recorded on an IR spectrophotometer with the Perkin-Elmer Spectrum 65 Fourier transform by the method of disturbed attenuation total reflection (ATR) in the frequency range 400–4000 cm–1. Microprobe analyses were carried out using a Carlo Erba EA 1108 Series CHN Elemental Analyzer (Center of Collective Use of IGIC RAS). Yield is calculated for the initial lanthanide salt.

2.2. Synthesis of complexes

*2.2.1. Synthesis of $[Gd_2(fur)_4(OAc)_2(phen)_2]{\cdot}4EtOH$ (**1**).* Hfur (0.22 g, 2 mmol) was added to a suspension of $Gd(OAc)_3{\cdot}3H_2O$ (0.12 g, 0.4 mmol) in 10 mL of acetonitrile and stirred for 1 h at 70 °C. A solution of phen (0.07 g, 0.4 mmol) in 5 mL of ethanol was carefully added. The resulting solution was kept at room temperature for one day. The formed white crystals were separated from the mother liquor by decantation. The yield was 0.25 g (90 %). Anal. calc. $C_{56}H_{58}Gd_2N_4O_{20}$: C 47.31, H 4.11, N 3.94. Found C 47.11, H 4.14, N 4.08. *FT-IR (ATR), ν/cm^{-1}:* 3419 w, 3145 w, 1696 w, 1580 s, 1541 s, 1502 s, 1418 s, 1361 s, 1207 m, 1144 m, 1105 w, 1068 w, 1006 w, 849 m, 811 m, 775 s, 724 s, 670 m, 600 m, 638 w, 548 w, 454 s, 415 w.

2.2.2 Synthesis of $[Gd_2(nfur)_6(phen)_2]{\cdot}4EtOH$ (2). Hnfur (0.31 g, 2 mmol) was added to a suspension of $Gd(OAc)_3{\cdot}3H_2O$ (0.12 g, 0.4 mmol) in 10 mL of acetonitrile and stirred for 1 h at 70 °C. A solution of phen (0.07 g, 0.4 mmol) in 5 mL of ethanol was carefully added. The resulting solution was kept at room temperature for one day. The formed white crystals were separated from the mother liquor by decantation. The yield was 0.3 g (83 %). Anal. Calc. $C_{62}H_{52}Gd_2N_{10}O_{34}$: C 41.47, h 2.91, N 7.80. Found C 41.48, h 2.68, N 7.68.FT-IR (ATR), ν/cm^{-1}: 3139 w, 1931 w, 1633 m, 1575 m, 1527 s, 1408 s, 1335 s, 1243 w, 1148 w, 1100 w, 1018 m, 960 w, 842 w, 811 m, 725 m, 672 w, 584 w, 491 s, 421 s

*2.2.3 Synthesis of $[Eu_2(fur)_4(OAc)_2(phen)_2]{\cdot}4EtOH$ (**3**).* Hfur (0.22 g, 2 mmol) was added to a suspension of $Eu(OAc)_3{\cdot}3H_2O$ (0.13 g, 0.4 mmol) in 10 mL of acetonitrile and stirred for 1 h at 70 °C. A solution of phen (0.07 g, 0.4 mmol) in 5 mL of ethanol was carefully added. The resulting solution was kept at room temperature for one day. The formed orange crystals were separated from the mother liquor by decantation. The yield was 0.2 g (75 %) anal. Calc. $C_{56}H_{58}Eu_2N_4O_{20}$: C 47.67, h 4.14, N 3.97. Found C 47.95, h 3.98, N 4.11.FT-IR (ATR), ν/cm^{-1}: 3135 w, 1582 s, 1543 s, 1502 s, 1418 s, 1361 s,1294 w, 1207 m, 1149 m, 1104 w, 1072 w, 1005 w, 965 w, 847 m, 810 m, 775 s, 724 s, 666 m, 602 m, 639 w, 551 w, 453 s, 417 w

*2.2.4 Synthesis of $[Eu_2(nfur)_6(phen)_2]{\cdot}4EtOH$ (**4**).* Hnfur (0.30 g, 2 mmol) was added to a suspension of $Eu(OAc)_3{\cdot}3H_2O$ (0.13 g, 0.4 mmol) in 10 mL of acetonitrile and stirred for 1 h at 70 °C. A solution of phen (0.07 g, 0.4 mmol) in 5 mL of ethanol was carefully added. The resulting solution was kept at room temperature for one day. The formed white crystals were separated from the mother liquor by decantation. The yield was 0.23 g (72 %). Anal. Calc. $C_{62}H_{52}Eu_2N_{10}O_{34}$: C 41.72, h 2.93, N 7.84. Found C 41.91, h 2.77, N 7.95. FT-IR (ATR), ν/cm^{-1}: 3133 w, 1933 w, 1701 w, 1690 m, 1635 m, 1568 m, 1525 s, 1408 s, 1337 s, 31,242 w, 1145 w, 1016 w, 1017 m, 960 w, 842 w, 812 m 780 s, 725 m, 673 w, 584 w, 488 s, 419 s

*2.2.5 Synthesis of $[Sm_2(3fur)_4(OAc)_2(phen)_2]{\cdot}2MeOH$ (**5**).* H3fur (0.22 g, 2 mmol) was added to a suspension of $Sm(OAc)_3{\cdot}3H_2O$ (0.13 g, 0.4 mmol) in 10 mL of acetonitrile and stirred for 1 h at 70 °C. A solution of phen (0.07 g, 0.4 mmol) in 5 mL of methanol was carefully added. The resulting solution was kept at room temperature for one day. The orange crystals were separated from the mother liquor by decantation. The yield was 0.2 g (75 %) anal. Calc. $C_{50}H_{38}Sm_2N_4O_{18}$: C 46.78, h 2.98, N 4.36. Found C 46.95, h 3.28, N 4.11. FT-IR (ATR), ν/cm^{-1}: 3135 w, 1582 s, 1543 s, 1502 s, 1418 s, 1361 s,1294 w, 1207 m, 1149 m, 1104 w, 1072 w, 1005 w, 965 w, 847 m, 810 m, 775 s, 724 s, 666 m, 602 m, 639 w, 551 w, 453 s, 417 w

*2.2.6 Synthesis of $[Sm_2(nfur)_6(phen)_2]$ (**6**). Method 1.* Hnfur (0.31 g, 2 mmol) was added to a suspension of $Sm(OAc)_3{\cdot}3H_2O$ (0.13 g, 0.4 mmol) in 10 mL of acetonitrile and stirred for 1 h at 70 °C. A solution of phen (0.07 g, 0.4 mmol) in 5 mL of ethanol was carefully added. The resulting solution was kept at room temperature for 1 day. The formed white crystals were separated from the mother liquor by decantation. The yield was 0.23 g (72 %). Anal. Calc. $C_{54}H_{28}Sm_2N_{10}O_{30}$: C 40.60, h 1.76, N 8.77. Found C 40.91, h 1.77, N 8.95. *FT-IR (ATR), ν/cm^{-1}:* 3617 w, 3135 w, 1723 w, 1642 s, 1602 m, 1574 s, 1409 s, 1322 s, 1242 m, 1201 w, 1148 w, 1018 w, 962 m, 842 s, 811 m 780 s, 724 s, 609 m, 581 m, 519 w, 489 s, 419 m

Method 2. $Sm_2(CO_3)_3{\cdot}4H_2O$ (0.07 g, 0.13 mmol) and Hnfur (0.118 g, 0.75 mmol) were dissolved in 15 mL H_2O at 80 °C for 1 h. The solution was filtered to remove the $Sm_2(CO_3)_3$ residue. Phen (0.045 g, 0.25 mmol) in 20 mL of MeCN was added to the resulting solution and stirred at 70 °C for 1 h. Then the reaction mixture was evaporated to dryness, the dry product was dissolved in 50 mL MeCN at a boil, the resulting solution was left for slow evaporation. Crystals suitable for X-ray diffraction analysis were separated by decantation, washed with cold MeCN, and dried in the air. The yield was 0.16 g (81 %). Anal. calc $C_{54}H_{28}Sm_2N_{10}O_{30}$: C 40.60, H 1.76, N 8.77. Found C 40.91, H 1.77, N 8.95.

*2.2.7 Synthesis of $[Sm_2(3fur)_6(phen)_2]{\cdot}H_2O$ (**7**).* $Sm_2(CO_3)_3{\cdot}4H_2O$ (0.14 g, 0.25 mmol) and H3Fur (0.17 g, 1.5 mmol) were dissolved in 15 mL H_2O at 80 °C for 30 min. Solution of phen (0.09 g, 0.5 mmol) in 20 mL of EtOH was added to the resulting solution. The resulting reaction mixture was stirred at 70 °C for 30 min, while a fine crystalline residue precipitated from the solution. Crystals suitable for X-ray diffraction analysis were obtained by slow evaporation of the mother liquor. The

yield was 0.23 g (72 %). Anal. Calc. $C_{54}H_{36}Sm_2N_4O_{19}$: C 48.20, h 2.70, N 4.17. Found C 48.41, h 2.77, N 4.25. FT-IR (ATR), ν/cm^{-1}: 3616 w, 3505 w, 3142 w, 3065 w, 2335 w, 1580 s, 1552 s, 1505 vs, 1420 vs, 1359 vs, 1206 s, 1150 s, 1105 w, 1074 m, 1005 m, 964 m, 848 m, 807 m, 773 vs, 726 vs, 636 m, 600 s, 553 m, 528 m, 448 vs

2.3. Crystallography

X-ray diffraction data for **1–7** were collected with a Bruker APEX2 diffractometer, using graphite monochromated Mo-Kα radiation (l = 0.71073 Å) [37]. A semiempirical adsorption correction has applied using the SADABS program [38]. Using OLEX2 [39], the structures were solved with the ShelXT [40] structure solution program using Intrinsic Phasing and refined with the XL refinement package using Least-Squares minimization against F^2 in anisotropic approximation for non-hydrogen atoms. Hydrogen atoms of OH-groups and those of water molecules were located from difference Fourier synthesis, positions of other hydrogen atoms were calculated, and they all were refined in isotropic approximation within the riding model. The geometry of polyhedra of metal atoms is determined using the SHAPE 2.1 program [41].

Crystal data and refinement parameters for **1–7** are given in Table S1-S2. The structural data of compounds **1–7** are deposited in the Cambridge Structural Data Bank (CCDC:2244013 (**1**), 2,244,014 (**2**), 2,244,015 (**3**), 2,244,016 (**4**), 2,244,017 (**5**), 2,244,018 (**6**), 2,244,019 (**7**) deposit@ccdc.cam.ac.uk.

2.4. Luminescence properties

For measuring the spectra of photoluminescence and optical excitation in the solid phase, a Horiba Jobin-Yvon Fluorolog QM-75–22-C spectrofluorometer was used. The instrument was equipped with a photomultiplier tube (PMT) detector, specifically the Hamamatsu R13456 PMT. A 75 W ArcTune xenon arc lamp served as the continuous excitation source. For measuring the spectra of photoluminescence and optical excitation in the solid phase, a Horiba Jobin-Yvon Fluorolog QM-75–22-C spectrofluorometer was used. The instrument was equipped with a photomultiplier tube (PMT) detector, specifically the Hamamatsu R13456 PMT. A 75 W ArcTune xenon arc lamp served as the continuous excitation source.

To measure the phosphorescence spectra in the visible spectral region for coordination compounds of Gd^{3+} ions with similar ligands, the same spectrofluorometer was used, but with an impulse xenon lamp as the excitation source. The samples were placed in quartz capillaries and cooled to 77 K using a cryostat filled with liquid nitrogen.

The decays of photoluminescence were also recorded using the Horiba Jobin-Yvon Fluorolog QM-75–22-C spectrofluorometer. In this case, an impulse xenon lamp with a frequency of 100 Hz and a pulse duration of 50 μs was used.

2.5. Spectroscopy and stability

The UV–vis spectra were obtained using Shimadzu UV-2600 spectrophotometer in, SoloPharm 0.9 % NaCl in the range of 220–600 nm. The stability of the complexes in solution was monitored by measuring the spectra of the sample for 48 h at room temperature.

2.6. Voltammetric study

Voltammograms (CVA) of the complex **7** were recorded on an AutoLab PGSTAT100 N (Metrohm, Zurich, Switzerland) potentiostat in a 10-mL three-electrode cell with a platinum wire counter electrode and a silver reference electrode (Ag/AgCl, KClsat). A reference electrode was attached to the electrolyte solution through a salt bridge containing a 0.1 M solution of n-Bu4NBF4 in acetonitrile. A platinum disk with an active surface area of 0.045 cm2 was used as a working electrode. The platinum electrode was polished with a suspension of Al2O3 (SPA 0.3) at a polishing set (Metrohm, Zurich, Switzerland) and washed with sulfuric acid and water with acetone. All solutions were thoroughly deaerated with argon. A solution of complex **7** was prepared in acetonitrile in a Schlenk vessel in an argon atmosphere. The concentration of the solution of complex 3 was 2.2 mM.

2.7. Antimycobacterial activity

To determine the biological activity of substances **1–7** possessing anti-tuberculosis properties in the *M. smegmatis mc² 155* test system, the paper disk method was used. The technique involved determining the size of the zone of inhibition of the growth of the strain seeded as a lawn on an agar medium, around paper disks containing the compound in various concentrations. The bacteria washed off Petri dishes with tryptone soya agar M−290 medium (Himedia) were grown overnight in Lemco-TW liquid medium (Lab Lemco' Powder 5 g/L (Oxoid), peptone special 5 g/L (Oxoid), NaCl 5 g/L, Tween- 80) at + 37 °C until the average logarithmic growth phase at optical density OD600 ¼ 1.5, then mixed with molten agar medium M−290 in a ratio of 1: 9: 10 (culture: Lemco-TW: M- 290) and the resulting mixture was poured as a top layer onto Petri dishes, 5 mL per dish, with 20 mL already solidified M−290 agar medium. After the agar in the top layer solidified, paper disks soaked with a solution of the test substance were placed on the plate surface. The culture was incubated for 24 h at + 37 °C. The diameter of the zone of inhibition of *M. smegmatis* growth around the paper disk impregnated with the compound was determined. The MIC (minimum inhibiting concentration) was taken as the concentration of the compound where the zone of growth inhibition was the smallest.

The most active compound **3** was examined for their activities *in vitro* against *M. tuberculosis* H37Rv by applying the resazurin microplate assay (REMA) as described previously [42–44]. The test compound **3** was dissolved in DMSO and added to 96-well plates in such a way that a range of test concentrations of 12.5 – 0.1 μg/mL would be obtained (two-fold serial dilutions).

3. Results and discussion

3.1. Synthesis

The synthesis was carried out by boiling of the aqueous acetates of Gd^{III}, Eu^{III}, Sm^{III} with furoic acids – 3-furoic (H3fur) or 5-nitro-2-furoic (Hnfur) in acetonitrile and subsequent adding an alcohol solution of 1,10-phenanthroline (phen) (Scheme 1). As a result, in the case of Hfur, an incomplete exchange of acetate anions for furoate anions occurs and isostructural complexes $[Ln_2(3fur)_4(OAc)_2(phen)_2]\cdot 4L$ (Ln = Gd (**1**), Eu (**3**), Sm (**5**); L =·EtOH (**2**, **4**), MeOH (**5**)) are formed. When aqueous lanthanide acetates interact with Hnfur and phen, a complete ion exchange occurs with the formation of complexes $[Ln_2(nfur)_6(phen)_2]\cdot 4L$ (Ln = Gd (**2**), Eu (**4**), Sm (**6**); L =·C_2H_5OH (**2, 4**)). Crystals suitable for X-ray diffraction analysis were obtained by slow diffusion of solutions.

Complex **6** was also obtained by reacting samarium carbonate $Sm_2(CO_3)_3\cdot 4H_2O$ with Hnfur in water followed by the addition of phen in MeCN solution. It should be noted that according to a similar procedure, it was possible to obtain the complex $[Sm_2(fur)_6(phen)_2]\cdot H_2O$ (**7**).

3.2. Crystal structure

All synthesized binuclear complexes **1–7** crystallize in a triclinic space group with an inversion center between lanthanide ions Ln1 and Ln1A and have a similar structure. The binuclear metalwork of complexes **1–7** is formed due to the coordination of two chelate-bridged OAc^- and two bridged fur^- anions (complexes **1**, **3**, **5**, (Fig. 1a)), two bridged and two chelated-bridged 3fur-anions (complex **7**, (Fig. 1b)) or two bridging and two chelate-bridging $nfur^-$anions (complexes **2**, **4**, **6** (Fig. 1c)). Each REE ion completes its environment to a "muffin"

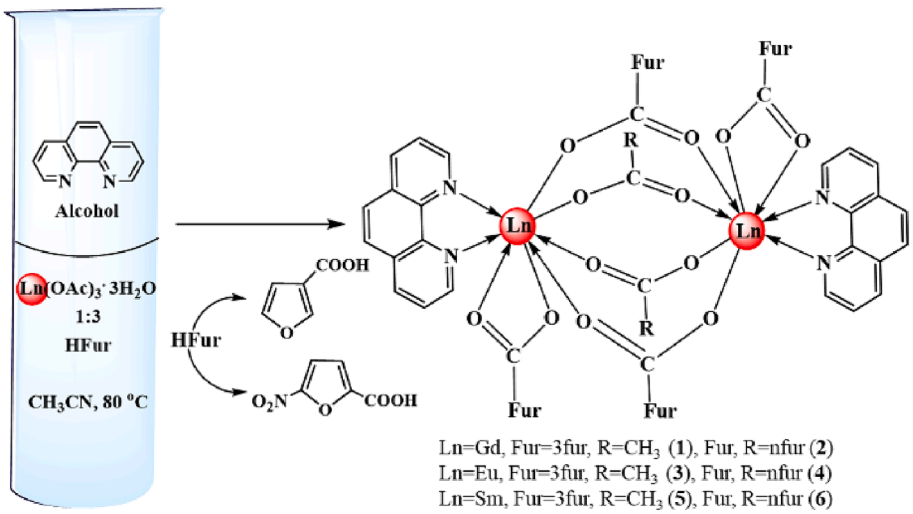

Scheme 1. Synthesis of 1–6.

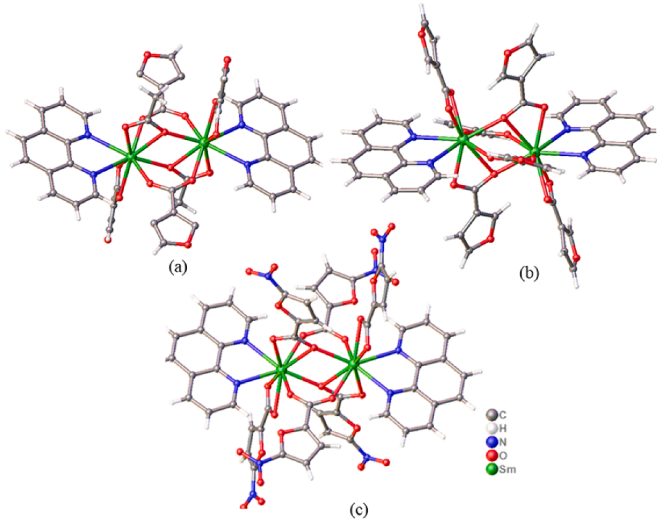

Fig. 1. Structure of **5** (a), **6** (b) and **7** (c). Solvate molecules are not shown.

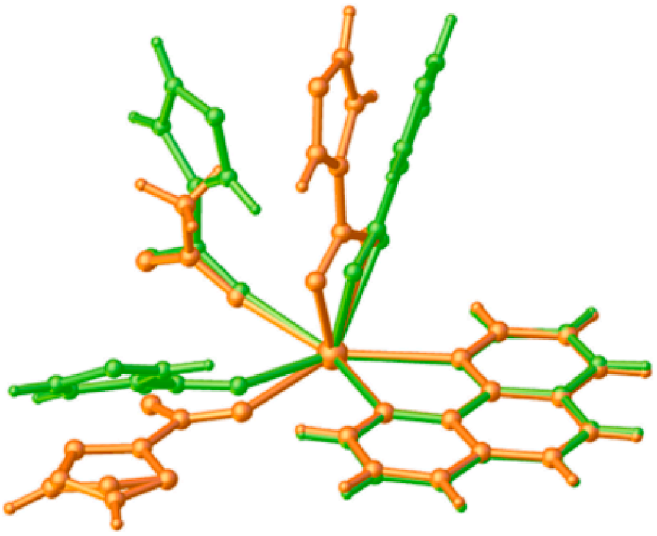

Fig. 2. Fragment overlay of complexes **5** (orange) and **7** (green). (For interpretation of the references to color in this figure legend, the reader is referred to the web version of this article.)

polyhedron due to the coordination of a chelated-bound fur$^-$ or nfur$^-$ anion and a phen molecule (Table S3). During the change Gd^{3+} ion to the Eu^{3+} and Sm^{3+} ions in complexes **1**, **3**, **5** and **2**, **4**, **6,** there is only a slight increase in the lengths of Ln–O, Ln–N bonds, as well as the distances Ln…Ln in the composition of binuclear metalcores (Table S4), whereas the geometry of the complexes and polyhedra of Ln^{3+} ions are preserved (Table S3).

Using the example of complexes **5** and **7**, it was shown that when replacing more compact acetate anions with fur-anions, small changes in the arrangement of substituents of fur-anions are observed (Fig. 2), which affects the system of non-covalent π···π interactions (Table S5), whereas in general the geometry of the binuclear molecule is preserved.

In crystal packages of complexes **1**–**7**, additional stabilization of crystal packages is observed due to the formation of a number of C—H…O interactions between hydrogen atoms of organic ligands and oxygen atoms of carboxyl groups and solvent molecules (Table S3, Fig S1). Solvate molecules of methanol, ethanol or water in the case of complexes **1**–**5**, **7** are embedded in the crystal lattice due to the formation of a system of hydrogen bonds with oxygen atoms of carboxyl groups and solvent molecules (Table S6).

Also, the molecules of the complexes are additionally interconnected due to the π – π-stacking interactions formed between pairs of coordinated phen molecules (complexes **1**–**7**), between pairs of 3fur$^-$ anions (**1, 3**), as well as between nfur-anions and phen molecules (**2, 4**). In the case of complexes with nfur$^-$ anions, there is a greater overlap and a significant reduction in the distances between the planes of phen molecules compared with 3-furoate complexes, which suggests that the interaction between pairs of phen molecules in this case is much higher in energy.

For complexes with nfur$^-$ anions, a significant number of N—O…π noncovalent interactions are observed (Table S7) with aromatic rings of nfur and phen. It is also possible to distinguish non-covalent interactions between NO_2 groups of nfur-anions of neighboring molecules (Table S8), which make a significant contribution to the stabilization of the crystal packages of the obtained complexes.

Thus, the molecules of the complexes are connected to each other due to numerous C—H…O, π – π, N—O…π and other non-covalent interactions, which leads to the formation of supramolecular layers in the crystal. (Fig.S1).

The obtained complexes **1–7** are isostructured to previously synthesized binuclear compounds with anions of 2-furoic (H2fur) or benzoic (HBA) acids of the composition $[Ln_2(2fur)_6(phen)_2] \cdot 2H_2O$ [45] and

$[Ln_2(BA)_4(OAc)_2(phen)_2]$ [46], the compounds have a similar structure with the preservation of the geometry of the metalost, the types of coordination of monocarboxylic acid anions and coordination polyhedra of metal ions. Only a slight increase in distances Ln…Ln can be noted for $[Eu_2(2fur)_6(phen)_2]\cdot 2H_2O$ and $[Eu_2(BA)_4(OAc)_2(phen)_2]$ up to 4.055 Å and 4.052 Å respectively.

3.3. Luminescence

To determine the energy of the first excited singlet level S_1 and triplet level T_1 of the phen and fur-ligands, coordination compounds of the Gd^{3+} ion with a completely similar ligand environment to complexes **3**, **5** and **4**, **6** were synthesized. The energy of the first excited singlet level S_1 was estimated from the long-wavelength edge of the band in the optical absorption spectrum by the tangent method. The energies of the S_1 level were of the order of 30700 cm^{-1} and 26700 cm^{-1} for complexes **1** and **2**, respectively.

The position of the triplet levels of most ligands from the phenanthroline class, known from the literature [47], are below the resonant level of the Gd^{3+} ion (~32000 cm^{-1}), which prevents direct energy transfer from the ligand to the Gd^{3+} ion. The absence of such transfer promotes radiative relaxation from the triplet state T_1 to the basic singlet state S_0 of the ligand. However, this transition is prohibited by the selection rules, which leads to a low emission intensity and relatively long lifetimes of the excited triplet state. Weak emission, moreover, competes with non-radiative relaxation. Thus, the time and resolved luminescence spectra of complexes **1** and **2** cooled to 77 K were recorded (Fig. 3).

The T1 energy of the ligand environment level of complexes **1** and **2** was estimated as a 0–0 phonon transition along the high-energy edge of the phosphorescence spectrum by the tangent method. The energies were 21,800 and 20200 cm^{-1} for complexes **1** and **2**, respectively. These values are comparable to the energy of the triplet level for the gadolinium complex of the composition described earlier $[Gd(phen)_2Cl_3(H_2O)_2]$ (22075 cm^{-1}) [48].

The optical excitation and luminescence spectra of complexes **3**–**6** in the solid phase at room temperature are presented on Fig. 4.

All studied complexes **3**–**6** exhibit ion-centered luminescence under optical excitation in a wide spectral range from 280 to 500 nm. At the same time, wide bands in the excitation spectra in the range from 280 to 400 nm are associated with the sensitization of luminescence through electronic transitions inside the ligand environment. Also, low-intensity narrow bands are observed in the excitation spectra corresponding to the direct excitation of Eu^{3+} and Sm^{3+} ions through the transitions $^7F_0 \rightarrow {}^5L_6$ (398 nm) and $^6H_{5/2} \rightarrow {}^6P_{3/2}$ (405 nm) respectively. This behavior indicates a relatively effective sensitization of luminescence precisely through the ligand environment. In the photoluminescence spectra for complexes **3** and **4**, spectral bands corresponding to electronic transitions are observed Eu^{3+}: $^5D_0 \rightarrow {}^7F_0$ (578–582 nm), $^5D_0 \rightarrow {}^7F_1$ (585–600 nm), $^5D_0 \rightarrow {}^7F_2$ (605–630 nm), $^5D_0 \rightarrow {}^7F_3$ (645–660 nm), $^5D_0 \rightarrow {}^7F_4$ (700–710 nm). Similar photoluminescence spectra were observed in the binuclear complexes of europium with anions of 2-furoic acid $[Eu_2(2fur)_4(phen)_2]\cdot H_2O$ [45], indicating a similar coordination polyhedron symmetry type. Moreover, the replacement of the furoate anion in binuclear complexes with anions of other aromatic acids (benzoate, methoxybenzoate) does not have a noticeable effect on the luminescence spectra [46,49].

Complexes **5** and **6** exhibit emission in the bands 570, 600 and 650 nm corresponding to the transitions $^4G_{5/2} \rightarrow {}^6H_J$ (J = 5/2, 7/2, 9/2, respectively) in the Sm^{3+} ion. Correlation of individual *f**-*f* transitions to spectral lines of Eu^{3+} and Sm^{3+} ions was carried out on the basis of literature data [50]. It is worth noting that no contributions from fluorescence and phosphorescence of the ligand environment are observed in the emission spectra of complexes **3** and **4**, which also indirectly indicates a relatively efficient transfer of electron excitation energy from the ligand donor to the acceptor ion. On the contrary, for complexes **5** and **6** in the 400–550 nm band, there is an intense contribution associated with the luminescence of the ligand environment, which indicates an incomplete energy transfer to the central Sm^{3+} ion. The ion-centered luminescence bands of complexes **3** and **4** are split due to the Stark effect. The splitting of the bands and the spectral arrangement of the transition barycenters practically coincide, which indicates an identical type of symmetry of the coordination polyhedron. Complexes **5** and **6** show similar behavior.

By the absolute method using an integrating sphere, overall quantum yield ($\mathbf{Q_{all}}$) was measured for all the compounds. For complexes **3**, **4**, and **6**, $\mathbf{Q_{all}}$ was 8.1, 2.1, and ~ 0.5 %, respectively.

Thus, the new synthesized complexes **3**–**6** demonstrate relatively efficient and bright ion-centered luminescence. The diagram in the XY color space (International Commission on Illumination, CIE 1931) for the emission of complexes **3**–**6** is presented on Fig. 5.

In the simplest case, the kinetics of luminescence is explained by a two-level model (relaxation of strictly one excited state) and obeys a mono-exponential law:

$$I(t) = I_0 \exp(-t/t_{obs})$$

where the observed attenuation time t_{obs} is defined as:

$$t\_obs = 1/k\_obs = 1/(k\_rad + k\_nrad)$$

k_{rad} и k_{nrad} – the rate constants of radiative and nonradiative relaxation, respectively.

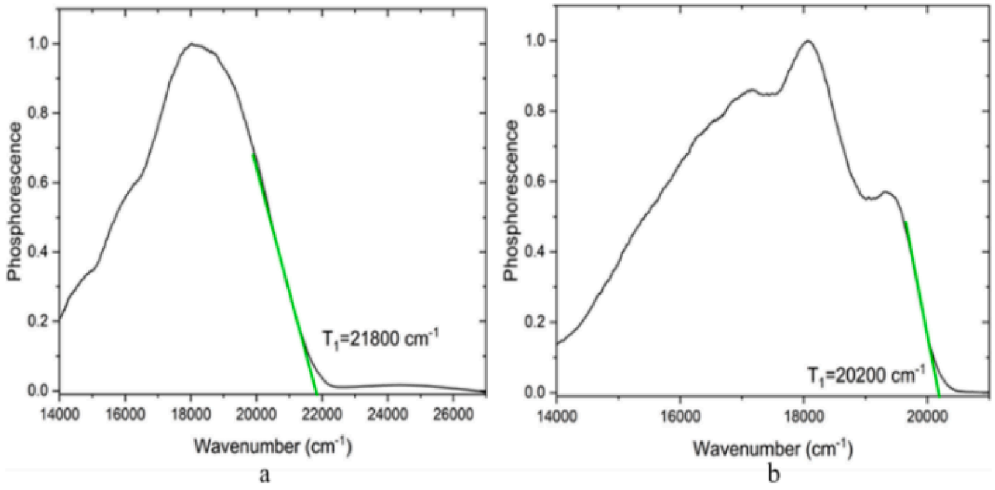

Fig. 3. Phosphorescence spectra in the energy representation of **1** (a) and **2** (b) at T = 77 K.

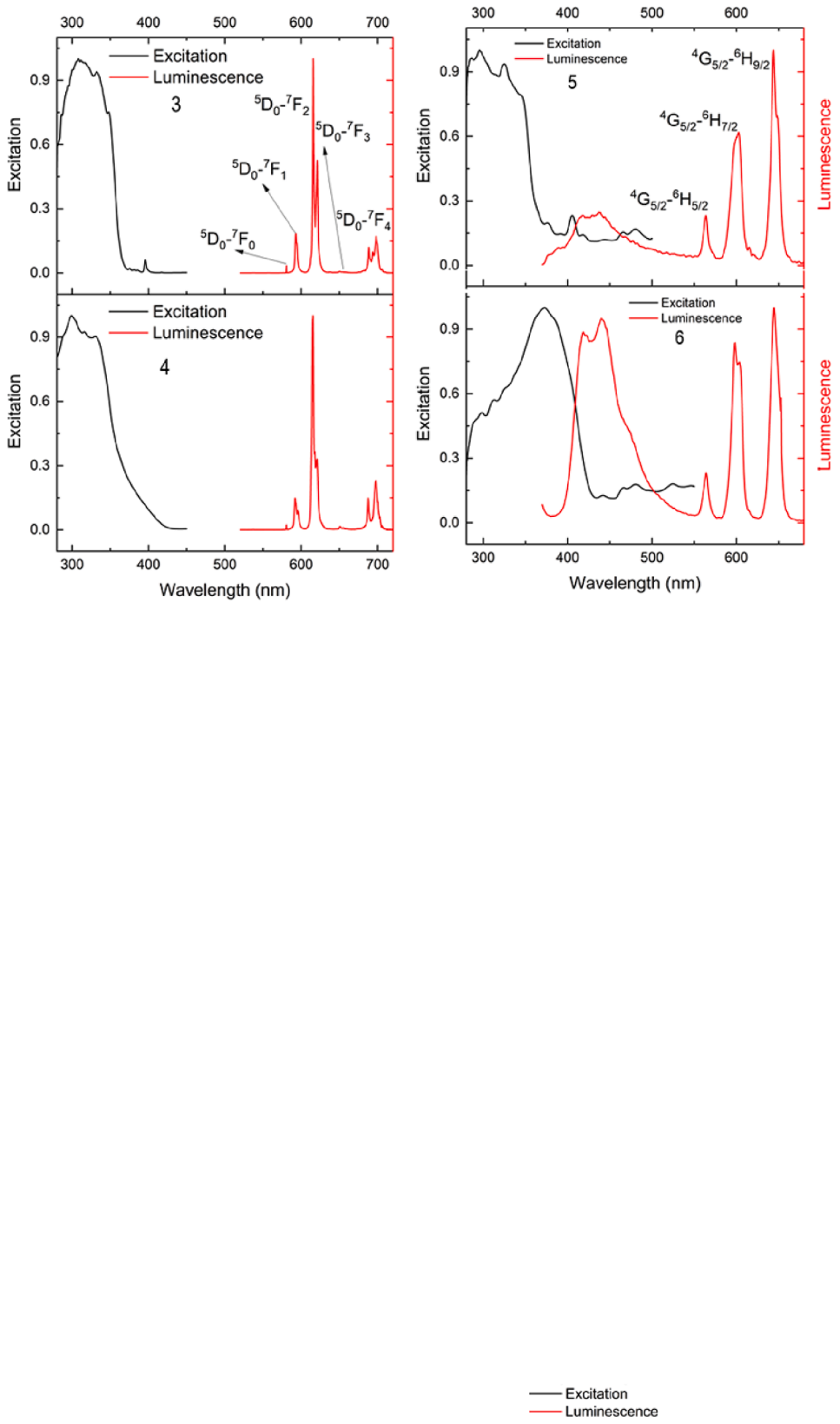

Fig. 4. Optical excitation and luminescence spectra for complexes **3**–**6** in the solid phase at $T = 300$ K. The registration wavelength is 615 nm (**3**, **4**) and 650 nm (**5**, **6**) when measuring the excitation spectrum. The wavelength of the excitation .
Source is 350 nm when measuring the luminescence spectrum

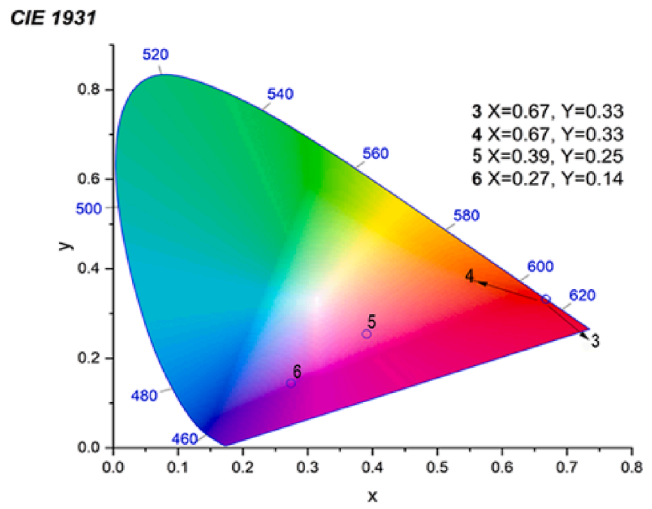

Fig. 5. Color diagram of the emission of complexes **3**–**6**.

The luminescence kinetics of the studied complexes in the solid phase under optical excitation through a ligand environment (380 nm), registered in the bands 612 nm (transition $^5D_0 \rightarrow {}^7F_2$ for complexes **3** and **4**) and 650 nm (transition $^4G_{5/2} \rightarrow {}^6H_{9/2}$ for **5** and **6**), are shown on Fig. 6. The luminescence kinetics of complex **3** was approximated by a mono-exponential function, while for complexes **4, 5** and **6**, the kinetics can be represented as a bi-exponential attenuation law. The lifetimes of the excited state calculated in this way are presented in Table 1. The lifetimes of Eu^{3+} and Tb^{3+} benzoate complexes $[Ln_2(phen)_2(BA)_4(OAc)_2]$ [46] are comparable to those of the complexes studied in this work. The energies of the ligand environment triplet level also show similarity.

From the experimental data presented above, a scheme of energy levels with possible ways of transmission and relaxation of the energy of electronic excitation in complexes **3**–**6** is constructed (Fig. 7).

During optical excitation of the studied complexes, electrons from the ground singlet state S^0 pass into the first excited singlet state S1. The S1 state can relax in two main ways: fluorescence and intercombination conversion (ISC). It is worth noting that for complexes **3** and **4**, the fluorescence of the ligand environment is not observed. The first excited triplet state can also relax in two main ways: phosphorescence and direct energy transfer to the central ion (ET). However, phosphorescence of the ligand environment is not observed for complexes **3–6**. After that, radiative relaxation is observed from the resonant levels of the central

Table 1
Luminescence attenuation times for crystal complexes **3**–**6** at room temperature.

Complex	t_{short}, ms	t_{long}, ms
3	–	1670
4	320	1000
5	30	70
6	40	90

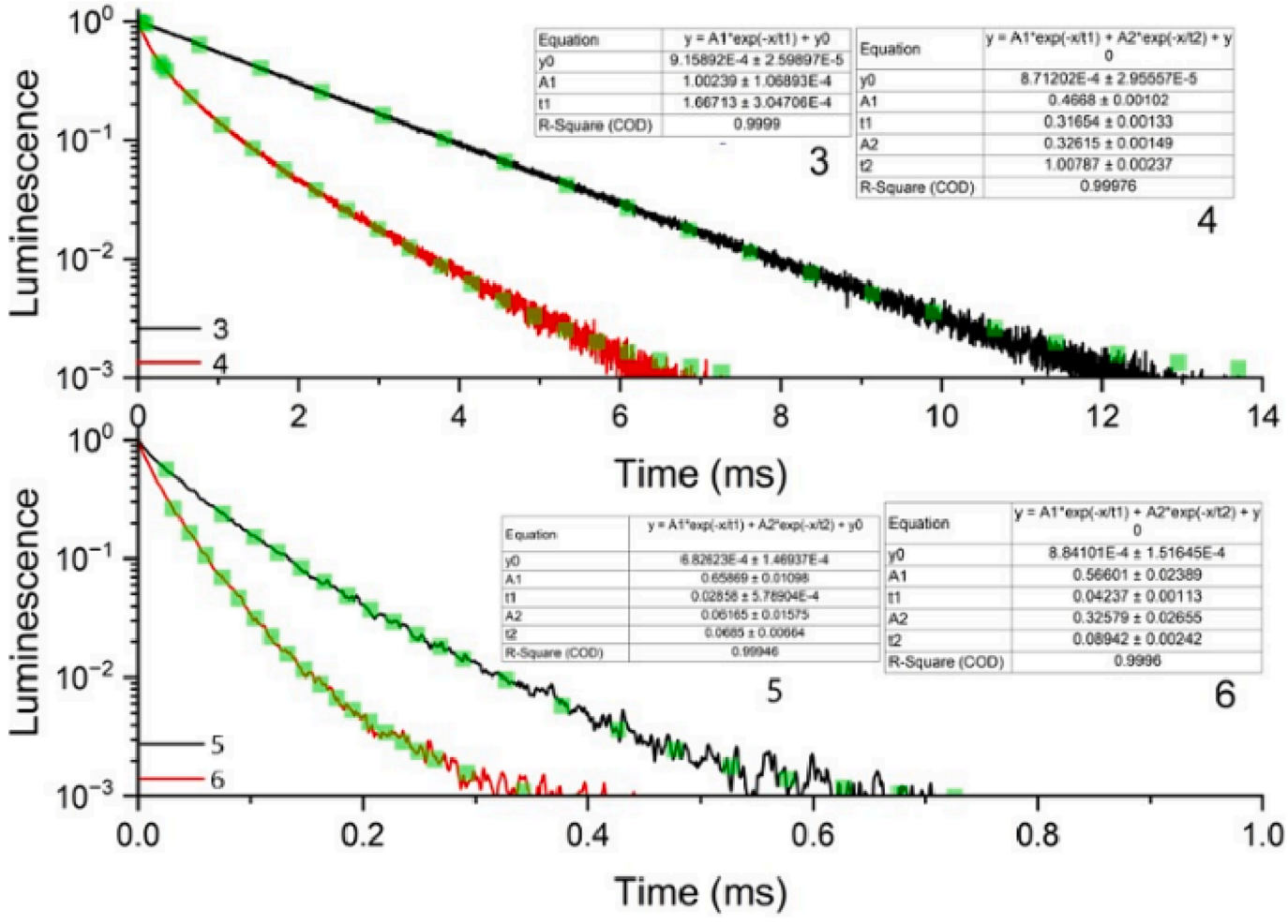

Fig. 6. The luminescence kinetics of the studied complexes in the solid phase under optical excitation of 380 nm, recorded in the bands 612 nm (**3** and **4**) and 650 nm (**5** and **6**).

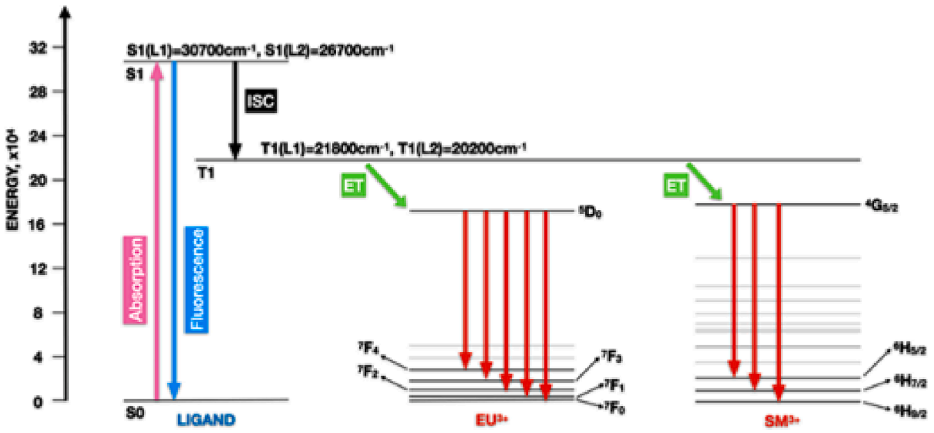

Fig. 7. Scheme of energy levels and possible ways of electron excitation energy transfer and relaxation for complexes **3**–**6**.

ions.

3.4. Uv–vis spectroscopy studies

For complexes **1**–**6**, the electronic absorption spectra of 1 were studied at a concentration of 10^{-5} M in saline solution (0.9 % NaCl) and 5 % glucose solution. The spectra were recorded for 48 h at room temperature (Fig. S2). The complexes have high absorption rates in the high energy region. The absorption band at 270 nm indicates effective intra–ligand π–π* and n-π* transitions within phen-ligands [51]. For all complexes, the low-intensity absorption band in the region of 300–350 nm is explained by the transfer of metal charge to the ligand (MLCT) [52]. Additional red-shift bands at a wavelength 325 nm are associated with the introduction of a nitro-group into the furoate anion in compounds 2, 4, 6.

3.5. Voltammetric study

Voltammetric study of binuclear samarium complex **7** was conducted in dimethylsulfoxide solution at glassy carbon electrode. No redox response was detected in the anodic potential range, whereas four consecutive irreversible reduction peaks (E_{pc} = − 2.12 V, −2.48 V, −2.63 V, −2.69 V vs. Fc^+/Fc) (Fig. 8) appeared in the cathodic scan.

Reduction of the metal centers ($Sm^{3+/2+}$) occurs first; the peak potential value is in good agreement with previously reported data for $Sm^{3+/2+}$ reduction in an aprotic media ($E_{1/2}$ = − 2.08 V vs. Fc^+/Fc for Sm(diaza-18-crown-6)Cl_3 in acetonitrile [53]). The significant anodic shift of the re-oxidation peak indicates the follow-up structural modification of the molecule. (E_{pa} = − 0.54 V) (Fig. 9a).

Notably, this follow-up modification of the reduced complex **7** is chemically reversible. This was confirmed by multiple cycling in the potential range including both the first reduction peak and the corresponding re-oxidation peak (−2.28 V − 0.47 V): the CV curves for different scans coincide well. With an increase in the potential scan rate up to 10 V/s, the number of electrons consumed at the first reduction peak is decreased and the reduction process becomes quasi-reversible (Fig. 9b). This is also accompanied by gradual diminishing of the oxidation peak at − 0.58 (Fig. 9b) corresponding to the modified complex. Thus, the first reduction process is best described within the ECE mechanism.

The anodic shift of the redox response of the $Sm^{3+/2+}$ redox couple in the modified complex evidences that the electron density at the Sm center is diminished. This is more likely attributed to the altering of the

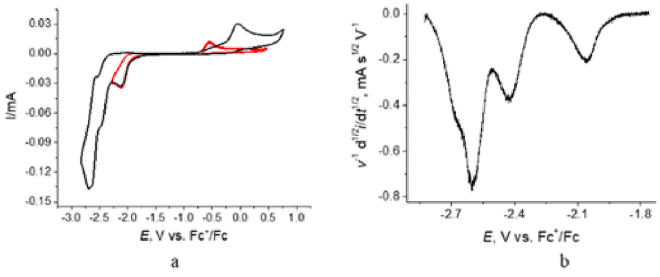

Fig. 9. (a) Multiple cycling in the potential range including first reduction peak of the complex **7** and the corresponding re-oxidation peak. Coincidence of the curves at different scans confirms chemical reversibility of the electrochemically induced coordination sphere rearrangement. (DMSO, GC, 100 mV/s); (b) potential scan rate dependence of the CV curve (semi-differential representation).

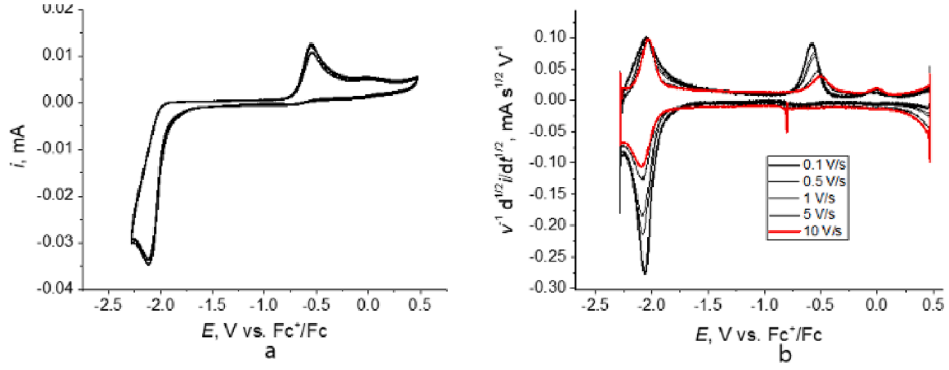

Fig. 8. Voltammogramm observed for complex **7** (0.1 M Bu_4NBF_4 in DMSO, GC electrode, 100 mV/s) (a) and its semi-differential representation (fragment corresponding to cathodic sweep) (b).

coordination mode of the one or more bridging carboxylate ligands (Scheme 2).

Notably, the rearrangement followed the one-electron transfer not only impedes re-oxidation of the Sm center which is reduced first, but also facilitates reduction of the remaining Sm^{3+} center. Thus, the rearrangement influences the coordination environment of the both samarium centers indicating that two μ^2-coordinated oxygen atoms in the bridging carboxylates participate in the rearrangement.

Further reduction leads to metallic samarium deposition at the electrode and free ligands release (re-oxidation peak of $Sm^{0/+3}$ at $E_{pa} = -0.04$ V vs. Fc^+/Fc is observed). The most cathodic peaks correspond to the reduction of the free phenanthroline ligands (the reduction peak potentials observed are in agreement with literature data: $E_{pc} = -2.54$ V и −2.72 V vs. Fc^+/Fc in DMF) [54].

3.6. Antibacterial activity

The antimicobacterial activity of the all obtained complexes was determined *in vitro* against non-*pathogenic M. smegmatis*, which are used as an object imitating *M. tuberculosis bacteria*, and are also used for primary screening of anti-tuberculosis drugs [55]. The criterion for selecting a compound is a minimum inhibitory concentration of <100 nmol/disc [56]. The results of the biological activity of the compounds *in vitro* were compared with the activity of rifampicin (Rif), a first-line drug for the treatment of tuberculosis under these experimental conditions. The concentration of the compound at which the minimum visible growth inhibition zone is observed is considered MIC (minimum inhibitory concentration, nmol/disc). The results of the study of antibacterial activity in the M. smegmatis mc2 155 test system and its changes over time for compounds **1**–**7** are shown in Table 2.

The diameter of the paper disk is 6 mm.

As can be seen from the table, the obtained complexes **1–7** exhibit high antimycobacterial activity comparable to anti–tuberculosis drugs – rifampicin and isoniazid. Complexes of europium **3** and **4** exhibit higher activity compared to complexes of samarium and gadolinium. It was previously shown that gadolinium polymer complexes with fur^- and $nfur^-$ anions have very high MIC values, which indicates their low bioactivity. The introduction of phen complexes significantly increases the activity of complexes against *M. smegmatis*. The same regularity was observed for *d*-metal complexes [26–32].

The complex **3**, which demonstrated the best activity against *M. smegmatis,* also has an antibacterial effect against *Mycobacterium tuberculosis* ($H37R_v$). The results of antibacterial activity (by REMA) **3** against *M. tuberculosis* H37Rv are shown in Table 3.

Table 2
The results of antimycobacterial activity against *M. smegmatis.*

Compounds	MIC, nmol/disk	The zone of inhibition, mm	
	24 h	24 h	120 h
1	**10**	6.43 ± 0.1	0
2	**10**	6.6 ± 0.17	6.2 ± 0
3	**5**	7. ± 0.5	6.9 ± 0.5
4	**6**	6.4 ± 0.25	6.2 ± 0.2
5	**12**	6.8 ± 0.29	6.5 ± 0.1
6	**13**	6.4 ± 0.29	6.2 ± 0.17
7	**15**	6.4 ± 0.12	6.1 ± 0.1
$[Gd(nfur)_3]_n$ [32]	1000	6.4 ± 0.3	0
$[Eu(fur)_3]_n$ [32]	2000	6.3 ± 0	6.1 ± 0.3
$[Gd(fur)_3]_n$ [32]	2000	6.4 ± 0	6.0 ± 0.3
$[Cu(fur)_2(phen)]$ [26]	5	6.3 ± 0	6.1 ± 0.3
$[Pd(fur)_2(phen)]$ [28]	50	6.8. ± 0.5	6.7 ± 0.5
$[Cu(phen)(CF_3CO_2)_2]$ [27]	10	6.4 ± 0	6.0 ± 0.3
Hfur	50	6.67 ± 0.29	6.1
Hnfur	25	0	0
phen	45	6.5 ± 0.06	0
Rif	5	6.5	6.5

Despite the fact that **3** showed a relatively low level of antibacterial activity against *Mycobacterium tuberculosis* H37Rv (MIC 12.5 μg/mL), the potential of this compound may be associated with activity against MDR and XDR-TB. However, the MIC of complex **3** is significantly lower than it of the previously studied complex $[Eu_2(HL)_3]$ (H_3L = 2,6-diformyl-4-methylphenol-di(benzoylhydrazone) [57]. Further study of the activity of **3** and its derivatives against clinical drug-susceptible and drug-resistant isolates of *M. tuberculosis* is required.

4. Conclusions

Here we shown that the reaction of lanthanide acetate, 3-furoic acid

Table 3
The results of antibacterial activity against *M. tuberculosis* $H37R_v$.

Compounds	Antibacterial activity against *M. tuberculosis* H37Rv(MIC) , μg/mL
3	12.5
$[Eu_2(HL)_3$*]	64
Isoniazid	0.2–0.4

* (H_3L = 2,6-diformyl-4-methylphenol-di(benzoylhydrazone).

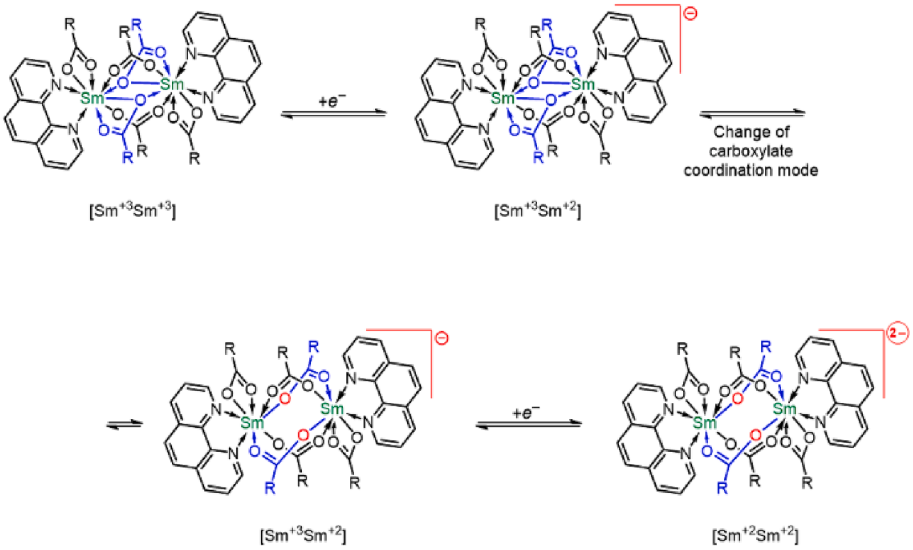

Scheme 2. The ECE process at the potential of the first reduction peak.

and −phen in ratio 1:3:1 leads to isostructural binuclear complexes $[Ln_2(3fur)_4(OAc)_2(phen)_2]$ (Ln = Sm, Eu, Gd) with incomplete exchange acetate anions. On the other hand, the use of 5-nitro-2-furoic acid instead of 3-furoic acid gave complexes $[Ln_2(nfur)_6(phen)_2]$. Crystal structure of the binuclear complexes is stabilized due to the formation of a number of C—H…O, N—O…π and π···π interactions. The photophysical properties of the complexes **1–6** were thoroughly investigated. The experimental results demonstrate the existence of a directed energy transfer channel from ligand donors to ion acceptors in the studied compounds. These compounds exhibit intense ion-centered luminescence when excited in a broad UV spectral range. The study of antibacterial properties **1–7** showed high activity of complexes *in vitro* against non-pathogenic *M. smegmatis*, comparable with rifampicin and isoniazid. The antibacterial activity against the reference strain *of M. tuberculosis* complex **3** was lower than isoniazid, but significantly exceeds the activity of lanthanide complexes described earlier in the literature. The obtained Eu^{3+} complexes can be useful for developing of bioimaging.

Author contributions

The manuscript was written through contributions of all authors.

CRediT authorship contribution statement

Marina A. Uvarova: Writing – original draft, Project administration, Methodology, Investigation, Funding acquisition, Conceptualization. **Marina E. Nikiforova:** Methodology. **Maxim A. Shmelev:** Investigation, Formal analysis. **Teimur M. Aliev:** Formal analysis. **Mikhail T. Metlin:** Writing – original draft, Visualization. **Ilya V. Taydakov:** Methodology, Formal analysis. **Olga B. Bekker:** Formal analysis. **Oleg A. Levitskiy:** Writing – original draft, Investigation. **Tatiana V. Magdesieva:** Validation, Methodology. **Gennady L. Rusinov:** Formal analysis. **Danila V. Belyaev:** Formal analysis. **Diana V. Vakhrusheva:** Investigation. **Svetlana Yu. Krasnoborova:** Investigation. **Mikhail A. Kiskin:** Writing – review & editing. **Irina A. Lutsenko:** Conceptualization. **Igor L. Eremenko:** Writing – review & editing, Supervision.

Declaration of competing interest

The authors declare that they have no known competing financial interests or personal relationships that could have appeared to influence the work reported in this paper.

Data availability

No data was used for the research described in the article.

Acknowledgements

This work was financially supported by the Russian Science Foundation (project No. 24-23-00188). We are gratefulto the User Facilities Center of Institute of General and Inorganic Chemistry of the Russian Academy of Sciences for physicochemical measurement

Appendix A

CCDC: 2,244,013 (**1**), 2,244,014 (**2**), 2,244,015 (**3**), 2,244,016 (**4**), 2,244,017 (**5**), 2,244,018 (**6**), 2,244,019 (**7**) contain the supplementary crystallographic data for this paper. These data can be obtained free of charge via http: //https://www.ccdc.cam.ac.uk.

Appendix B. Supplementary data

Supplementary data to this article can be found online at https://doi.org/10.1016/j.ica.2024.122066.

References

[1] Y. Louie, T.J. Meade, A cobalt complex that selectively disrupts the structure and function of zinc fingers, Proc. Natl Acad. Sci. USA 95 (1998) 6668.
[2] S. Rojas, E. Quartapelle-Procopio, F.J. Carmona, M.A. Romero, J.A.R. Navarro, E. Barea, Biophysical characterisation, antitumor activity and MOF encapsulation of a half-sandwich ruthenium (II) mitoxantronato system, *J. Mater. Chem. B.* 2 (2014) 2473.
[3] C.B. Scarim, R.L. de Farias, N.A.V. de Godoy, C.M. Chin, J.L. Dos Santos, F. R. Pavan, Recent advances in drug discovery against Mycobacterium tuberculosis: Metal-based complexes, European Journal of Medicinal Chemistry. 214 (2021) 113166.
[4] N.J. Bello-Vieda, H.F. Pastrana, M.F. Garavito, A.G. Ávila, A.M. Celis, et al., Antibacterial activities of azole complexes combined with silver nanoparticles, Molecules. 23 (2018) 361.
[5] H.U. Rashid, M.A.U. Martines, J. Jorge, P.M. de Moraes, M.N. Umar, K.H. Khan, Cyclen-based Gd3+ complexes as MRI contrast agents: Relaxivity enhancement and ligand design, Bioorgan. Med. Chem. 4 (2016) 5663.
[6] A. Babič, V. Vorobiev, C. Xayaphoummine, G. Lapicorey, A.S. Chauvin, L. Helm, E. Allémann, Self-Assembled Nanomicelles as MRI Blood-Pool Contrast Agent, Chem-Eur. J. 24 (2018) 1348.
[7] J. Wang, R. Wang, J. Yang, Z. Zheng, M.D. Carducci, T. Cayou, N. Peyghambarian, G.E. Jabbour, First oxadiazole-functionalized terbium (III) β-diketonate for organic electroluminescence, J. Am. Chem. Soc. 123 (2001) 6179.
[8] C.R. De Silva, J.F. Wang, M.D. Carducci, S.A. Rajapakshe, Z.P. Zheng, Synthesis, structural characterization and luminescence studies of a novel europium (III) complex [Eu (DBM) 3 (TPTZ)](DBM: dibenzoylmethanate; TPTZ: 2, 4, 6-tri (2-pyridyl)-1, 3, 5-triazine), Inorg. Chim. Acta. 357 (2004) 630.
[9] J.-C.-G. Bünzli, C. Piguet, Taking advantage of luminescent lanthanide ions, Chem. Soc. Rev. 34 (2005) 1048.
[10] C.R. De Silva, J.R. Maeyer, A. Dawson, Z. Zheng, Adducts of lanthanide β-diketonates with 2, 4, 6-tri (2-pyridyl)-1, 3, 5-triazine: Synthesis, structural characterization, and photoluminescence studies, Polyhedron. 26 (2007) 1229.
[11] J.-C.-G. Bünzli, Rising stars in science and technology: Luminescent lanthanidematerials, Eur. J. Inorg. Chem. 5058 (2017).
[12] S.I. Weissman, Intramolecular energy transfer the fluorescence of complexes of europium, J. Chem. Phys. 10 (1942) 214.
[13] S. Dasari, S. Singh, S. Sivakumar, A.K. Patra, Dual-Sensitized Luminescent Europium(III) and Terbium(III) Complexes as Bioimaging and Light-Responsive Therapeutic Agents, Chem. Eur. J. 22 (2016) 17387.
[14] S. Aime, S.G. Crich, E. Gianolio, G.B. Giovenzana, L. Tei, E. Terreno, High sensitivity lanthanide(III) based probes for MR-medical imaging, Coord. Chem. Rev. 250 (2006) 1562.
[15] J.-C.-G. Bünzli, Lanthanide luminescence for biomedical analyses and imaging, Chem. Rev. 110 (2010) 2729.
[16] X. Wang, H. Chang, J. Xie, B. Zhao, et al., Recent developments in lanthanide-based luminescent probes, Coord. Chem. Rev. 273 (2014) 201.
[17] G. Bao, Lanthanide complexes for drug delivery and therapeutics, Journal of Luminescence. 228 (2020) 117622.
[18] Y. Li, F. Guo, S. Wei, D. Li, J. Zhang, K. Xu, D. Li, Heterobimetallic lanthanide tetrahedral cages: Synthesis, design and application for potential multimodal imaging contrast agent, Journal of Rare Earths. 42 (2) (2024) 278.
[19] T.A.F. Reji, A.J. Pearl, B.A. Rosy, Synthesis, characterization, cytotoxicity, DNA cleavage and antimicrobial activity of homodinuclear lanthanide complexes of phenylthioacetic acid, Journal of Rare Earths. 31 (10) (2013) 1009.
[20] M.T. Kaczmarek, M. Zabiszak, M. Nowak, R. Jastrzab, Lanthanides: Schiff base complexes, applications in cancer diagnosis, therapy, and antibacterial activity, Coord. Chem. Rev. 370 (2018) 42.
[21] Q.-L. Guan, Y.-H. Xing, J. Liu, W.-J. Wei, X. Wang, F.-Y. Bai, Application of multiple parallel perfused microbioreactors: Synthesis, characterization and cytotoxicity testing of the novel rare earth complexes with indole acid as a ligand, J. Inorg. Biochem. 128 (2013) 57.
[22] Y. Ning, M. Zhu, J.L. Zhang, Near-infrared (NIR) lanthanide molecular probes for bioimaging and biosensing, Coord. Chem. Rev. 399 (2019) 213028.
[23] V. Tsaryuk, K. Lyssenko, K. Zhuravlev, V. Zolin, V. Kudryashova, I. Pekareva, Z. Klemenkova, Influence of ligand architecture on the structure of coordination centre in dimeric europium carboxylates with 1, 10-phenanthroline, Journal of Rare Earths 27 (4) (2009) 539.
[24] E. Echenique-Errandonea, A. Zabala-Lekuona, J. Cepeda, A. Rodríguez-Diéguez, et al., Effect of the change of the ancillary carboxylate bridging ligand on the SMM and luminescence properties of a series of carboxylate-diphenoxido triply bridged dinuclear ZnLn and tetranuclear Zn2Ln2 complexes (Ln= Dy, Er), Dalton Trans. 48 (2019) 190.
[25] M.A. Kiskin, E.A. Varaksina, I.V. Taydakov, I.L. Eremenko, Synthesis, structure and luminescence of {Zn2Ln(OH)}(Ln= Eu, Gd, Tb) complexes with a triangular metal core, Inorg. Chim. Acta. 482 (2018) 85.
[26] I.A. Lutsenko, D.E. Baravikov, M.A. Kiskin, Y.V. Nelyubina, et al., Bioisostere modifications of Cu2+ and Zn2+ with pyromucic acid anions and N-donors: synthesis, structures, thermal properties, and biological activity, Russ. J. Coord. Chem. 46 (2020) 411.
[27] M.A. Uvarova, I.A. Lutsenko, M.A. Shmelev, S.E. Nefedov, et al., Research of the influence of anions in complexes [CuPhen(Hpz)2X2](X= CF3COO−, Otf−, Cl−) on the structure and bioactivity, New J Chem. 48 (2) (2024) 717.
[28] I.A. Lutsenko, D.E. Baravikov, M.A. Kiskin, et al., Bioisostere modifications of Cu2 + and Zn2+ with pyromucic acid anions and N-donors: synthesis, structures, thermal properties, and biological activity, Russ. J. Coord. Chem. 46 (2020) 411.

[29] M.A. Uvarova, I.A. Lutsenko, K.A. Babeshkin, A.V. Sokolov, et al., Solvent effect in the chemical design of coordination polymers of various topologies with Co2+ and Ni2+ ions and 2-furoate anions, CrystEngComm 25 (48) (2023) 6786.
[30] M.P.C. Campello, E. Palma, I. Correia, P.M. Paulo, et al., Lanthanide complexes with phenanthroline-based ligands: Insights into cell death mechanisms obtained by microscopy techniques, Dalton Trans. 48 (2019) 4611.
[31] E. Bartolomé, J. Bartolomé, A. Arauzo, J. Luzón, L. Badía, R. Cases, et al., Antiferromagnetic single-chain magnet slow relaxation in the {Tb(α-fur)3}n polymer with non-Kramers ions, J. of Mater. Chem. c. 22 (2016) 5038.
[32] M.A. Uvarova, I.A. Lutsenko, M.A. Shmelev, O.B. Bekker, M.A. Kiskin, I. L. Eremenko, Furancarboxylate Coordination Polymers of Gd3+ and Eu3+: Synthesis, Structural Variations, and Biological Properties, Russ. J. Coor. Chem. 49 (9) (2023) 555–564.
[33] P.A. Demakov, V.P. Fedin, Synthesis and structure of new europium (III) and terbium (III) coordination polymers with trans-1, 4-cyclohexanedicarboxylic acid, Russian Chemical Bulletin 71 (5) (2022) 967–973.
[34] Zaguzin A S, Bondarenko M A, Abramov P A, Rakhmanova M I, Sokolov, M N, Fedin, V. P., & Adonin, S. A. (2022). Two-Dimensional and Three-Dimensional Coordination Polymers Based on Ln (III) and 2, 5-Diiodoterephthalates: Structures and Luminescent Behavior. *Inorganics*, 2022; *10*(12), 262.
[35] B.V. Bukvetskii, A.S. Shishov, A.G. Mirochnik, Crystal structures of three centrosymmetric TbIII complexes. Structural model for triboluminescence, Russian Chemical Bulletin 72 (6) (2023) 1307–1321.
[36] A.S. Zaguzin, P.A. Abramov, M.I. Rakhmanova, A.N. Usoltsev, M.N. Sokolov, V. P. Fedin, S.A. Adonin, Luminescent sensors based on Ln (III) 2, 5-diiodotereph-thalate coordination polymers, Polyhedron 116908 (2024).
[37] Smart, (control) and SAINT (integration). Software. Version 5.0, Bruker AXS Inc., Madison (WI, USA), 1997.
[38] L. Krause, R. Herbst-Irmer, G.M. Sheldrick, D. Stalke, Comparison of silver and molybdenum microfocus X-ray sources for single-crystal structure determination, J. Appl. Cryst. 48 (2015) 3.
[39] O.V. Dolomanov, L.J. Bourhis, R.J. Gildea, J.A.K. Howard, H. Puschmann, OLEX2: a complete structure solution, refinement and analysis program, J. Appl. Crystallogr. 42 (2009) 339.
[40] A.L. Spek, Structure validation in chemical crystallography, Acta Crystallogr. d. 65 (2009) 148.
[41] D. Casanova, M. Llunell, P. Alemany, S. Alvarez, The rich stereochemistry of eight-vertex polyhedra: a continuous shape measures study, Chem. Eur. J. 11 (2005) 1479.
[42] J.-C. Palomino, A. Martin, M. Camacho, H. Guerra, et al., Resazurin microtiter assay plate: simple and inexpensive method for detection of drug resistance in *Mycobacterium tuberculosis*, Antimicrob. Agents Chemother. 46 (2002) 2720.
[43] N.K. Taneja, J.S. Tyagi, Resazurin reduction assays for screening of anti-tubercular compounds against dormant and actively growing Mycobacterium tuberculosis, Mycobacterium bovis BCG and Mycobacterium smegmatis, J. Antimicrob. Chemother. 60 (2007) 288.
[44] G.A. Sadykhov, D.V. Belyaev, D.V. Vakhrusheva, N.I. Eremeeva, et al., New Approach to Biologically Active Indolo[2,3-b]quinoxaline Derivatives through Intramolecular Oxidative Cyclodehydrogenation, Chem. Select. 7 (2022) 18.
[45] X. Li, L. Jin, S. Lu, J. Zhang, Synthesis, structure and luminescence property of the ternary and quaternary europium complexes with furoic acid, Journal of Molecular Structure. 604 (2002) 65.
[46] X. Meng, X. Liu, L. Zhang, J. Zhou, H.H. Zou, J. Zhang, X. Zou, A series of new lanthanide benzoates: Syntheses, crystal structures, and luminescent properties, Dyes and Pigments. 201 (2022) 110182.
[47] B. Yan, H. Zhang, S. Wang, J. Ni, Intramolecular energy transfer mechanism between ligands in ternary rare earth complexes with aromatic carboxylic acids and 1,10-phenanthroline, J. Photochem. Photobiol. a: Chem. 116 (3) (1998) 209.
[48] L.N. Puntus, K.A. Lyssenko, M.Y. Antipin, J.C. Bünzli, Role of inner-and outer-sphere bonding in the sensitization of EuIII-luminescence deciphered by combined analysis of experimental electron density distribution function and photophysical data, Inorg. Chem. 47 (23) (2008) 11095.
[49] R.X. Ma, Z.M. Chen, Z.H. Gao, S.P. Wang, R.F. Wang, J.J. Zhang, Synthesis, structures and properties of ternary rare earth complexes with m-methoxybenzoic acid and 1,10-phenanthroline, Synthetic Metals. 159 (13) (2009) 1272.
[50] Spectra and energy levels of rare earth ions in crystals. Interscience.Publishers, New York (1968).
[51] Ö. Dağlı, D.A. Köse, O. Şahin, Z.S. Şahin, The synthesis and structural characterization of transition metal coordination complexes of coumarilic acid, J. Therm. Anal. Calorim. 128 (2017) 1373.
[52] J. Toigo, G. Farias, C.A.M. Salla, T.A. Duarte, et al.Speeding-up thermally activated delayed fluorescence in Cu(I) complexes using aminophosphine ligandsEur. J. Inorg. Chem.31772021Ö. Dağlı, D.A. Köse, O. Şahin, Z.S. Şahin, The synthesis and structural characterization of transition metal coordination complexes of coumarilic acid, J. Therm. Anal. Calorim. 128 (2017) 1373.
[53] I. Marolleau, J.P. Gisselbrecht, M. Gross, F. Arnaud-Neu, M.J. Schwing-Weill, Solvent effects on thermodynamic and electrochemical parameters: lanthanide cryptates in acetonitrile, Dalton Trans 4 (1990; () 1285.
[54] M. Magni, A. Colombo, C. Dragonetti, P. MussiniSteric vs electronic effects and solvent coordination in the electrochemistry of phenanthroline-based copper complexesElectrochim. Acta.1412014324I. Marolleau, J.P. Gisselbrecht, M. Gross, F. Arnaud-Neu, M.J. Schwing-Weill, Solvent effects on thermodynamic and electrochemical parameters: lanthanide cryptates in acetonitrile, Dalton Trans. 4 (1990) 1285.
[55] S. Ramón-García, C. Ng, H. Anderson, J.D. Chao, X. Zheng, T. Pfeifer, Y. Av-Gay, M. Roberge, C.J. ThompsonSynergistic drug combinations for tuberculosis therapy identified by a novel high-throughput screenAntimikrob. Agen. Chemother.5520113861M. Magni, A. Colombo, C. Dragonetti, P. Mussini, Steric vs electronic effects and solvent coordination in the electrochemistry of phenanthroline-based copper complexes, Electrochim. Acta. 141 (2014) 324.
[56] O.B. Bekker, D.N. Sokolov, O.A. Luzina, N.I. Komarova, et al., Synthesis and activity of (+)-usnic acid and (−)-usnic acid derivatives containing 1,3-thiazole cycle against, Mycobacterium tuberculosis. Med. Chem. Res. 24 (2015) 2926.
[57] K. Das, S. Nandi, S. Mondal, T. Askun, Z. Cantürk, P. Celikboyun, T. Akitsu, Triply phenoxo bridged Eu (III) and Sm (III) complexes with 2, 6-diformyl-4-methylphe-nol-di (benzoylhydrazone): structure, spectra and biological study in human cell lines, New J Chem 39 (2) (2015) 1101.